

SIMULATION OF EX-VESSEL MELT JET BREAKUP AND SENSITIVITY ON MODEL PARAMETERS AND ACCIDENT CONDITIONS

Kiyofumi Moriyama¹ and Hyun Sun Park^{1*}

¹ Division of Advanced Nuclear Engineering
Pohang University of Science and Technology (POSTECH)
77 Cheongam-ro, Nam-gu, Pohang, Gyeongsangbuk-do, Korea
khmoriym@postech.ac.kr; hejsunny@postech.ac.kr

ABSTRACT

The breakup of a melt jet falling in a water pool and the coolability of the melt particles produced by such jet breakup are important phenomena in terms of the mitigation of severe accident consequences in light water reactors, because the molten and relocated core material is the primary heat source that governs the accident progression.

We applied a modified version of the fuel-coolant interaction simulation code, JASMINE, developed at Japan Atomic Energy Agency (JAEA) to a plant scale simulation of melt jet breakup and cooling assuming an ex-vessel condition in the APR1400, a Korean advanced pressurized water reactor. Also, we examined the sensitivity on 5 model parameters and 5 initial/boundary condition variables.

The results showed that the melt cooling performance of a 6 m deep water pool in the reactor cavity is enough for removing the initial melt enthalpy for solidification, for a melt jet of 0.2 m initial diameter. The impacts of the model parameters were relatively weak and that of some of the initial/boundary condition variables, namely the water depth and melt jet diameter, were very strong. A significant fraction of the melt was not broken up and formed a continuous melt pool on the containment floor in cases with a large melt jet diameter or a shallow water pool.

KEYWORDS

Severe accident, Ex-vessel debris coolability, Melt jet breakup, Sensitivity analysis

1 INTRODUCTION

During a severe accident of light water reactors (LWRs) involving significant core damage and melt down, the molten and relocated core material is the primary heat source that governs the accident progression. Securing coolability of the molten core is the crucial factor for the mitigation of impacts of the accident. Except the case that dry-cavity strategy is taken, it is likely that the molten core, when it penetrates the lower head of the reactor vessel (RV), drops into a water pool in the reactor cavity that is prepared as an accident management (AM) action or as a result of coolant leakage from the reactor cooling system (RCS). Thus, it is highly concerned whether the molten core in such conditions is broken up into small particles and makes

*Corresponding author

a coolable debris bed or makes an agglomerated melt lump that leads to inefficient cooling and the molten core concrete interaction (MCCI)[1, 2].

The melt jet breakup phenomena have been intensively studied in the last decades. However, the major activities in this field rather focused on the energetic steam explosion and the melt jet breakup was included as the premixing phase of the phenomena[3]. Thus, the priority in model development for the melt jet breakup was put in the early phase, up to several seconds, and in transient distribution of the materials in the premixture. Also, some phenomenological aspects can be treated parametrically or by bounding (conservative) approaches, in case difficulties are encountered in putting enough confidence in using mechanistic models[4].

JASMINE[5] is a fuel-coolant interaction (FCI) simulation code developed at Japan Atomic Energy Agency (JAEA) and available at OECD/NEA Databank. It has been validated to some extent for the assessment of steam explosion energetics. However, its application to long term melt jet breakup and cooling behavior has not been tested comprehensively. It needs consideration on additional factors in the melt jet behavior that was worked around by parametric approaches or out of the scope in considering short time range till the triggering of steam explosions. Such aspects include the size distribution of the melt particles, agglomeration of melt particles when it falls on the floor, and so on.

In our recent work[6], we introduced additional models into JASMINE, including an empirical model for the particle size distribution and an improved model for the settlement and agglomeration of the particles on the floor, and tested the modified code by simulating experiments, namely ALPHA/GPM series with alumina-zirconia mixture or steel melt jet by JAEA[7] and FARO melt jet quenching experiments with $\text{UO}_2\text{-ZrO}_2$ mixture by JRC Ispra[8].

In this work, we applied the modified version of JASMINE to the plant scale simulation of the ex-vessel melt jet breakup and cooling in a geometry assuming the APR1400, a Korean advanced pressurized water reactor, and examined the influences of model parameters and initial/boundary conditions.

2 JASMINE CODE AND ADDITIONAL MODELS

Figure 1 shows the concept of melt jet breakup modeling in JASMINE. The model consists of a two-phase flow solver and a set of melt models including a vertical one dimensional jet, Lagrangian grouped particles and a radial one dimensional pool. The melt pool model accommodates a molten pool or solidified continuous lump on the floor. All those models are configured for 2D cylindrical geometry. The heat transfer from the high temperature melt is mainly carried by the particle model for it has most of the surface area of the melt. Liu-Theofanous (1996)[9] correlation for film boiling on spherical particles and the Stefan-Boltzmann law for radiation heat transfer are the most important models in this aspect.

The following additional models were implemented in the previous work[6].

- Empirical correlation for the melt particle size distribution
- Simplified non-local (beyond cell) radiation heat transfer model
- Improved model consistency on the settlement of melt particles on the floor and merge into the melt pool
- Corrected initial horizontal velocity of the melt particles after produced by the melt jet breakup

The modified version of JASMINE code was tested by simulation of selected experimental data, and the simulation reproduced the overall behavior observed in the experiments well for the cases the water pool

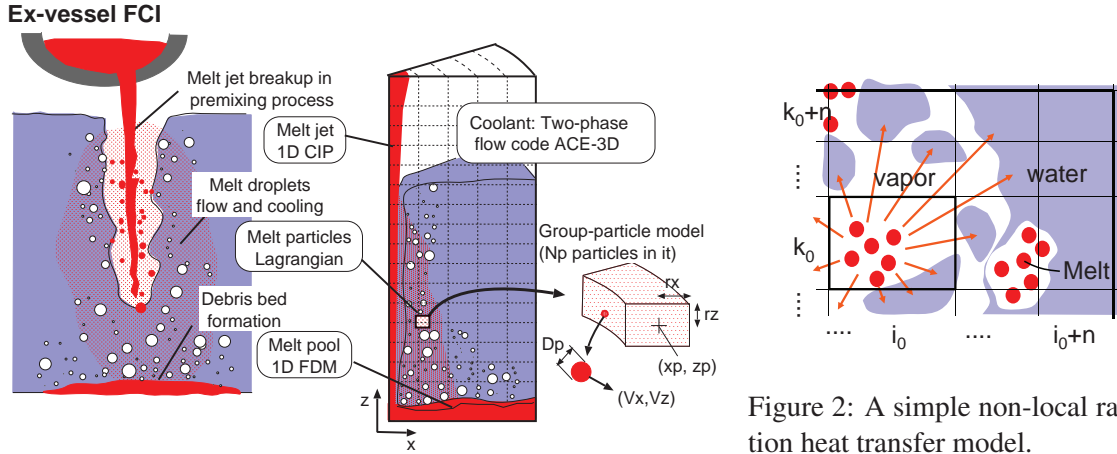


Figure 1: Modeling of melt jet breakup in JASMINE code.

had subcool and the void fraction in the pool was not very high. The major part of the added models are briefly described in the followings.

Empirical correlation for particle size distribution

An empirical correlation by Moriyama et al.[7] was implemented. It was developed based on their experiments with alumina-zirconia mixture or steel melt (APHA/GPM series) at JAEA[7], FARO experiments with corium (urania-zirconia mixture) melt at JRC Ispra[10, 11], PREMIX experiments with alumina at Forschungszentrum Küste (FZK)[12] and so on. They showed experimental data for these various melt materials were well correlated by Rosin-Rammler distribution[13]

$$F = 1 - \exp\left\{-\left(D_p/D_e\right)^n\right\}, \quad (1)$$

with the distribution constant $n = 1.5$, where F is the cumulative mass fraction of particles smaller than size D_p . The absolute size constant, D_e , is related to the mass median diameter, D_{MM} , by $D_{MM} = D_e(\log 2)^{1/n}$. The empirical correlation for the mass median diameter was expressed with Bond number based on the particle diameter, $Bo_p \equiv g\rho_m D_{MM}^2/\sigma_m$, by

$$Bo_p^{1/2} = F_{sb}(\rho_v/\rho_l)^{1/3}(\rho_l/\rho_m)^{2/3} \quad (2)$$

$$F_{sb} = 25\{2.2 - \exp(-13N_{sb})\} \quad (3)$$

$$N_{sb} = c_{pl}\Delta T_{sub}/\Delta h_{fg}, \quad (4)$$

where g , ρ_v , ρ_l , ρ_m , σ_m , c_{pl} , Δh_{fg} and ΔT_{sub} are the gravitational acceleration, the vapor, water and melt densities, melt surface tension, water specific heat and latent heat of evaporation, and subcooling, respectively.

Non-local radiation heat transfer

Oxide melt surfaces with relatively high emissivity, ~ 0.8 , and of high temperatures 2000–3000K release significant part of the heat as thermal radiation with peak wavelength $\sim 1\mu\text{m}$ (Wien's displacement law) that penetrates into 1–10cm order of depth in water and much more in vapor[14, 15]. With typical mesh sizes for FCI simulations, $\sim 10\text{cm}$, water can be regarded as opaque object for radiation absorption and vapor is transparent. Practically in FCI simulations, it often happens that void fraction in the cell where melt particles reside becomes very large, e.g. > 0.5 , and the radiation heat transfer partially reaching into adjacent cells

is plausible. However, conventionally the constitutive models including heat transfer is confined locally in each cell. When a too strong heat source appears in a cell where only small amount of heat sink, e.g. liquid water, exists, it may also cause numerical problems.

Figure 2 shows the concept of a simple model for the non-local deposition of the radiation heat. The radiation heat release in a cell (i_0, k_0) is deposited in the local and neighboring cells $(i = i_0 - n \cdots i_0 + n; k = k_0 - n \cdots k_0 + n)$ according to the distance from the source cell, $r_0(i, k)$, and the void fraction in each cell, $\alpha_{i,k}$. The local deposition fraction in the source cell is given by $f_a(\alpha_0)$, where α_0 is the void fraction in the source cell and the function, f_a , for the fraction of absorption is given as follows.

$$f_a(\alpha) = \begin{cases} 1 & (\alpha \leq 0.3) \\ (0.95 - \alpha)/0.65 & (0.3 < \alpha \leq 0.95) \\ 0 & (0.95 < \alpha) \end{cases} \quad (5)$$

In the surrounding cells up to the n -th adjacent, the rest of the heat is deposited by the weight of water existence and the inverse square of the distance from the source cell. The fraction of deposition in cell i, k is expressed by

$$\{1 - f_a(\alpha_0)\} f_{wi,k} / \sum_{p,q \neq i_0, k_0} f_{wp,q} \cdot \quad (6)$$

The weight function, $f_{wi,k}$, is defined by

$$f_{wi,k} = f_a(\alpha_{i,k}) V_{i,k} / r_0(i, k)^2 \quad (7)$$

where $V_{i,k}$ is the fluid volume in the cell i, k . The default range of the cell layers considered is $n = 2$.

3 ANALYSIS CONDITION

3.1 Assumed Plant Type, Geometry and Accident Condition

We assumed a late phase severe accident condition in the APR1400, an advanced pressurized water reactor developed by Korea Electric Power Corporation (KOPEC) and Korea Hydro and Nuclear Power Company (KHNP), being constructed as Shin-Kori units 3 & 4 in Korea and Barakah units 1 & 2 in UAE (as of 2015).[17] This type of reactor adopts severe accident management measures including the “flooded cavity” aiming at cooling and retention of damaged and molten core inside the reactor vessel by flooding the reactor cavity to submerge the bottom of the reactor vessel (in-vessel retention by external reactor vessel cooling, IVR-ERVC). A large amount of water, $\sim 2470 \text{ m}^3$, stored in the in-containment refueling water storage tank (IRWST) is used for that purpose. Information on the geometry of the reactor cavity, relevant severe accident conditions can be obtained from Kim et al. (2005)[18], Park et al. (2011)[19] and Rempe et al. (2005)[20] as summarized in Table 1.

Figure 3 shows the analytical model for the geometry of the APR1400 reactor cavity. The actual reactor cavity is asymmetric and consists of relatively narrow vertical part below the reactor and a horizontal duct for the instrumentation cables that has a floor area of 80 m^2 [19]. This was modeled by a 2-dimensional cylindrical domain preserving the floor area. A constant pressure was given as a boundary condition at the top of the domain. The containment has a large volume, $\sim 94700 \text{ m}^3$, and the expected pressure rise due to the quench of the maximum amount of the molten core, $\sim 145 \text{ t}$, is not so high, $\sim 0.1 \text{ MPa}$. Then, setting a constant pressure boundary rather than modeling whole the containment volume is a reasonable approach.

Table 1: Geometry and accident condition relevant to APR1400 severe accident.

| | | |
|--|-----------|--|
| Radius of the reactor vessel lower head (m) | 2.5 | Geometry information through Kim et al. (2005), Park et al. (2011). |
| Reactor cavity depth (m) | 6.5 | |
| Cavity floor area (m ²) | 80 | |
| Free volume of the containment (m ³) | 94700 | |
| In-vessel molten core pool mass (t) | 120-145 | Severe accident analysis results through Rempe et al. (2005), Ahn et al. (2012). |
| Molten core temperature (K) | 2900-3300 | |
| Pressure in the cavity (MPa) | ~0.19 | |
| Pressure in the reactor vessel (MPa) | Low | |
| Water level in the cavity (m) | 1-6 | |
| Water temperature in the cavity (K) | ~304 | |

Table 2: Physical properties of the melt material.[16]

| | |
|--|-------------|
| Liquidus/Solidus temperature (K) | 2850 / 2830 |
| Density (liq/sol) (kg/m ³) | 7960 / 9430 |
| Specific heat (liq/sol) (J/kg K) | 565 / 445 |
| Latent heat of fusion (MJ/kg) | 0.362 |
| Surface tension (liq) (N/m) | 0.45 |
| Emissivity | 0.79 |

Composition: UO₂-ZrO₂ 80:20 wt%

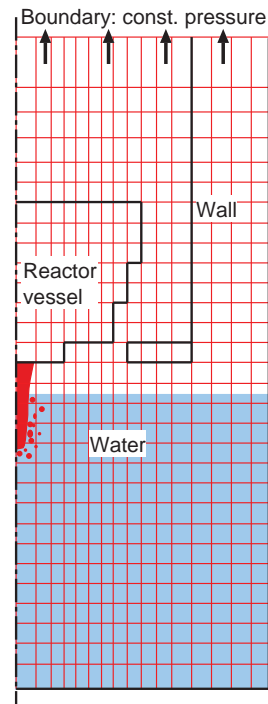


Figure 3: Analytical grid for APR1400 ex-vessel melt jet breakup and quenching.

The thermohydraulic condition during various severe accident sequences were considered based on existing severe accident analyses results for the APR1400 through Rempe et al. (2005)[20] and Ahn et al. (2011)[21]. Analyses of middle–small cold leg break loss of coolant accident (LOCA) and station black out (SBO) with loss of feed water sequences with SCDAP/RELAP-3D and SCDAP/RELAP5 codes by Idaho National Engineering and Environmental Laboratory (INEEL) and Korea Atomic Energy Research Institute (KAERI), respectively, showed similar results[20]: molten core mass in the lower head of the reactor vessel 120–145 t and the molten core temperature 2900–3300 K. The pressure in the reactor vessel was high for the SBO sequence. However, it was likely that a creep rupture of the pressurizer surge line due to hot steam flow would reduce the pressure. Ahn et al.[21] reviewed severe accident analyses for Shin-Kori units 3 & 4 by KHNP and referred for setting parameters in their ex-vessel steam explosion analyses. The condition in the reactor cavity was pressure below 0.2 MPa, water temperature about 300 K and water level 1.2–6.4 m.

The melt material according to those analyses[20, 21] was mostly a mixture of UO₂ and ZrO₂ and involved up to 10wt% of metal Zr. We used material properties for 80wt% UO₂-20wt% ZrO₂ mixture available from Annunziato et al.[16] as given in Table 2.

3.2 Model Parameters and Initial/Boundary Conditions

Table 3 shows the list of model parameters and initial/boundary condition variables related to the melt jet breakup and cooling behavior, and their values for the base case calculation and for sensitivity analyses. The sensitivity analysis cases are hereafter referred to by the names as indicated in the right end column. Description of the meaning and significance of 5 model parameters examined here is given as follows.

Table 3: Model parameters and initial/boundary conditions in the base case and sensitivity analyses.

| Parameter | Base case (BC) value | Modified value | Case ID |
|---|----------------------|----------------|-----------|
| Factor for jet breakup length ^{*1} , C_{ent} | 1 | 0.7 / 1.5 | JB1 / JB2 |
| Factor for particle size ^{*2} , C_{dmm} | 1 | 0.7 / 1.5 | PS1 / PS2 |
| Factor for heat transfer ^{*3} , C_{htc} | 2 | 1 / 4 | HT1 / HT2 |
| Coefficient for T_{sf} criteria for particle merge to pool, f_{tcr} (merge if $T_{sf} > T_{sol} + f_{tcr}(T_{liq} - T_{sol})$) | 0 | -0.5 / 0.5 | PM1 / PM2 |
| Particle group production criteria ^{*4} , N_{pcr} , n_{hist} | 10000, 500 | 4000, 200 | NP |
| Melt initial temperature (K), T_j (Superheat) | 3010 (170) | 3300 (460) | MT |
| Melt jet diameter (m), D_j | 0.2 | 0.5 | MD |
| Melt jet velocity (m/s), V_j | 6 | 12 | MV |
| Water level (m), H_p | 5.9 | 1.1 / 3.1 | WL1 / WL2 |
| Water temperature (K), T_l (Subcool) | 300 (92) | 350 (42) | WT |

*1 Modifies the melt stripping mass flux on the jet surface (larger values make shorter jet breakup lengths)

*2 Modifies the mass median diameter of particles *3 Modifies heat transfer coefficients for particles

*4 Particle groups are released when the number of particles $> N_{pcr}$ or the elapsed time steps $> n_{hist}$

C_{ent} : A modification factor for the jet breakup length. It actually multiplies the melt entrainment volume flux, V_e , that is evaluated by the jet breakup length given by the correlation: $V_e = C_{ent}(V_{Ji}/2)(D_{Ji}/L_{brk}^*)$, where the asterisk means the value by an empirical correlation. Thus, the jet breakup length obtained as a calculation result becomes $1/C_{ent}$ times of the value given by the correlation: $L_{brk} = L_{brk}^*/C_{ent}$. It directly affects the amount of melt that reaches the floor without breakup when the jet breakup length is longer than the water pool depth.

C_{dmm} : A modification factor for the mass median diameter, D_{MM} , of the melt particles produced by jet breakup. It gives a strong impact on the surface area, thus the heat transfer rate.

C_{htc} : A modification factor for heat transfer coefficients for melt particles. The base case value, 2, is based on the best estimate results in simulation of experiments in the previous study.[6]

f_{tcr} : A coefficient for the surface temperature criteria for particle merge to pool. The settled particles merge into the melt pool or the solidified lump on the floor when $T_{sf} > T_{sol} + f_{tcr}(T_{liq} - T_{sol})$, where T_{sf} , T_{sol} and T_{liq} are the surface temperature of melt particles, solidus and liquidus points of the melt, respectively. The fraction of the melt that is first broken up into particles and re-agglomerates on the floor can be sensitive to this parameter.[6]

N_{pcr}, n_{hist} : Criteria for particle group generation from the jet surface. The “pre-particle group buffers” at the jet surface, the model to store the entrained melt mass temporarily in every time step, are checked and released as particle groups when the number of particles exceeds N_{pcr} or the elapsed time step exceeds n_{hist} . They change the scale of the particle groups that influences the total number of particle groups, and the computational resource usage. Simulation of experiments (~ 100 kg melt) is available with $N_{pcr} = 2000$ and $n_{hist} = 100$. A plant scale simulation needs larger numbers.

Among the initial/boundary condition variables, we picked up 5 variables as described below. They were determined according to the relevant accident conditions summarized in Table 1.

T_j : Initial melt temperature, i.e. the enthalpy of the melt.

D_j, V_j : The diameter and velocity of the melt jet at the inlet. They determine the flow rate of the melt and the rate of the thermal energy input into the system. The diameter is determined by the possible hole size in the lower head of the reactor vessel. The local creep failure was suggested by Rempe et al.[20] as a plausible vessel failure mode. We set 0.2 m hole diameter as the base case and tested 0.5 m as maximum. The velocity depends on the liquid level and back pressure in the reactor vessel. Considering that relatively low pressure is likely, we assumed up to 1 MPa of the pressure and liquid level corresponding to the maximum mass, 145 t. It derives 5–16 m/s. We set 6 m/s for the base case and the twice larger for sensitivity analysis.

H_p : The water level is important as available space for the melt jet breakup and mixing with water. Also, our previous study on steam explosions[22] showed its impact on the explosion loads; shallow water pools are good for mitigation of the steam explosion energetics.

T_l : The water temperature. The subcool of water enhances the heat transfer.

Note that completely quenching the whole amount of the melt assumed in the reactor vessel, ~145 t, corresponds to 2.3×10^5 MJ and equals the apparent plus latent heat of ~90 t water. It corresponds to about 1.1 m deep water pool with the given floor area 80 m^2 . It is the same as the assumed pool depth in the case WL1.

4 RESULTS AND DISCUSSIONS

4.1 Overall Behavior

Figures 4–7 show material profile snapshots in the base case, BC, and selected cases, MD, MV and WL1 in which distinct differences of the behavior were observed. The cases with increased melt inlet flow rates, MD and MV, showed larger oscillating void pockets around the falling jet column and stronger swirl of water that rolls upward in the middle to peripheral zone of the pool. The case with a shallow pool, WL1, showed only limited part of the melt jet was broken up.

4.2 Mass and Heat Exchange History

Figure 8 (a) and (b) show the histories of total mass in the system and transferred heat, respectively. Release of 145 t of melt takes long time, 95 s, for the base case, 47 s for MV and 15.3 s for MD. Thus, only the case with a large jet diameter, MD, showed the completion of the melt fall during the calculation time of 20 s as shown in Fig. 8 (a). The heat transfer behavior showed almost linear increase of the transferred heat. The nearly constant heat transfer rates indicate that quasi steady state structures for heat transfer were established during the melt jet fall. Considering this observation of quasi steady state and required computational resource, we limited the simulation time till 20 s and examined the heat transfer performance in the quasi steady state.

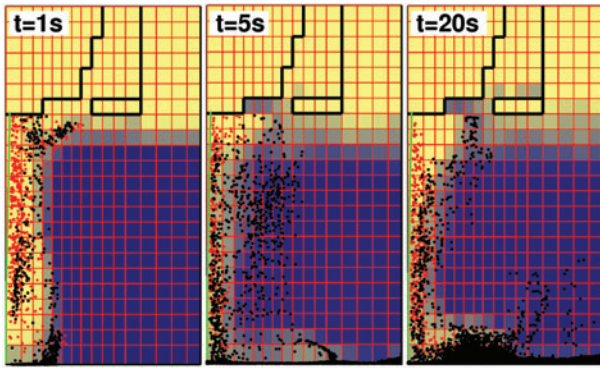


Figure 4: Snapshots of BC (Base case) (time 1,5,20s) (Red/black dots are molten/frozen particles).

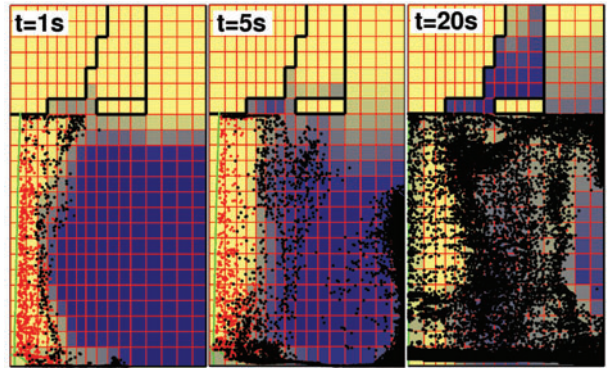


Figure 5: Snapshots of MD (Large jet) (time 1,5,20s) (Red/black dots are molten/frozen particles).

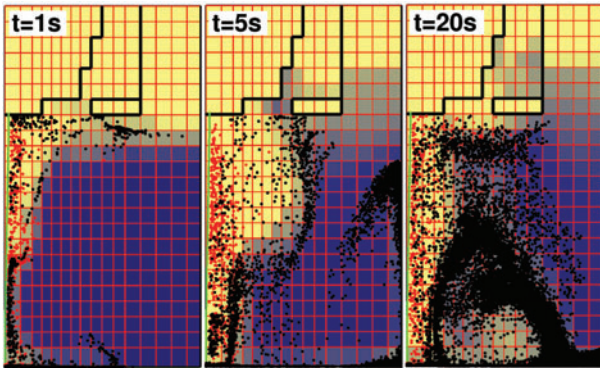


Figure 6: Snapshots of MV (Fast inlet) (time 1,5,20s) (Red/black dots are molten/frozen particles).

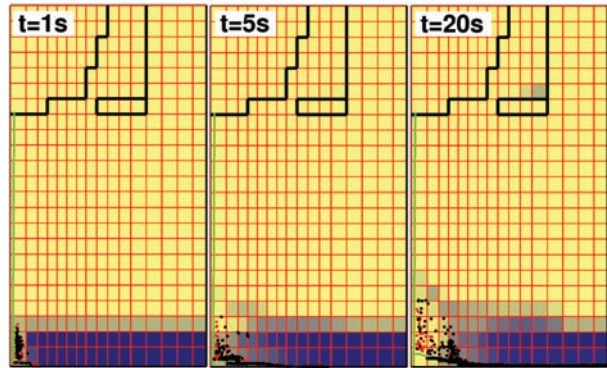


Figure 7: Snapshots of WL1 (Shallow pool) (time 1,5,20s) (Red/black dots are molten/frozen particles).

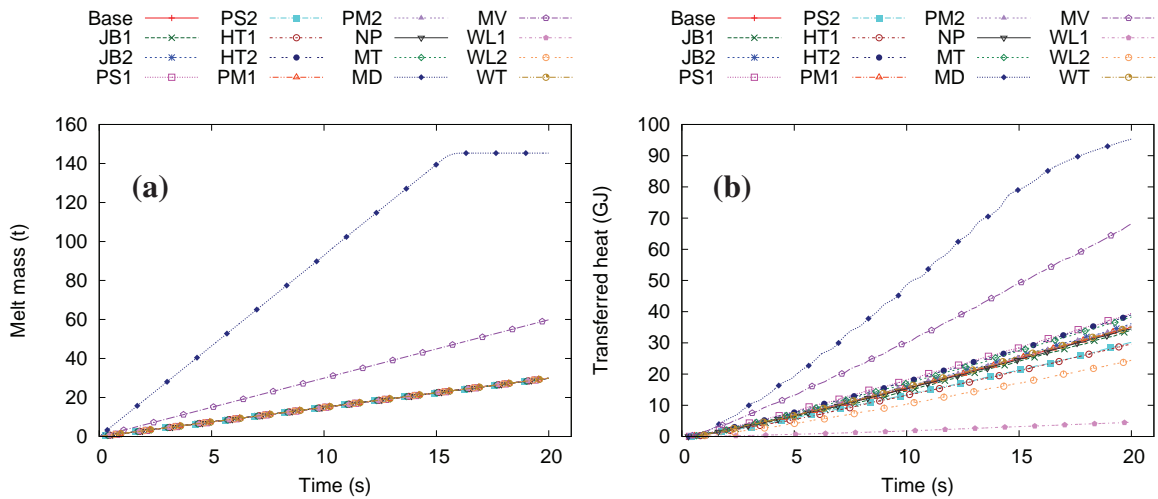


Figure 8: Total melt mass (a) and heat transferred from melt to water (b).

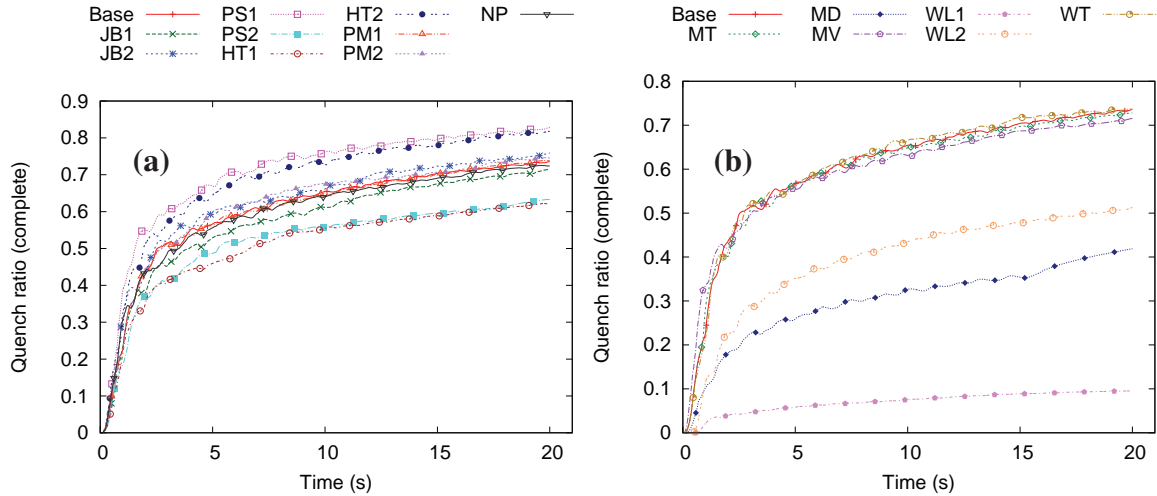


Figure 9: Quench ratio, (heat exchanged)/(enthalpy for complete quench to the room temperature (300 K)); (a) influence of model parameters, (b) influence of initial/boundary conditions.

4.3 Quench Ratio

The ratio of the heat transferred from the melt to water and the total enthalpy brought by the melt can be used as an index for the heat transfer performance. By using two different scales for the melt enthalpy, we evaluated the following indexes.

- Quench ratio in terms of complete cooling: $Q_{ex}/\Delta H_{300K}$ where Q_{ex} is the heat transferred from melt to water, ΔH_{300K} is the total enthalpy brought in by the melt with 300K as the base temperature, and
- Quench ratio in terms of solidification: $Q_{ex}/\Delta H_{sol}$ where ΔH_{sol} is the total enthalpy brought in by the melt with the solidus point as the base temperature.

Figure 9 shows the quench ratio in terms of complete cooling with the sensitivity on the model parameters (a) and on the initial/boundary conditions (b). The base case showed the ratio ~ 0.74 at 20 s, rapidly increasing in the initial stage ~ 5 s and later slow increase. Other cases also showed qualitatively similar trends indicating a quasi steady state balance of incoming and exchanged heat of the melt for the time scale of the melt fall. For the value of unity means the temperature of whole the melt equalized to the water initial temperature, 300K, the values are always less than 1. For the given range of the sensitivity variables, the impact of the initial/boundary conditions (Fig. 9 (b)) were more significant than that of the model parameters (Fig. 9 (a)). Especially the melt jet diameter (MD) and the water level (WL1, WL2) showed strong influences.

Figure 10 shows the quench ratio in terms of solidification with the sensitivity on the model parameters (a) and on the initial/boundary conditions (b). The values more than unity mean that the average enthalpy of the melt in the system is below the enthalpy at the solidus point. Thus, this index indicates the average state of the melt material, i.e. still molten or already solidified. The base case result and most of the other cases showed values more than 1 at 20 s, except the case WL1 in which only small part of the melt was broken up (Fig. 7) and the quench ratio was ~ 0.33 . Compared with the complete quench ratio (Fig. 9), the case of modified melt temperature (MT) showed more significant difference from the base case (Fig. 10 (b)).

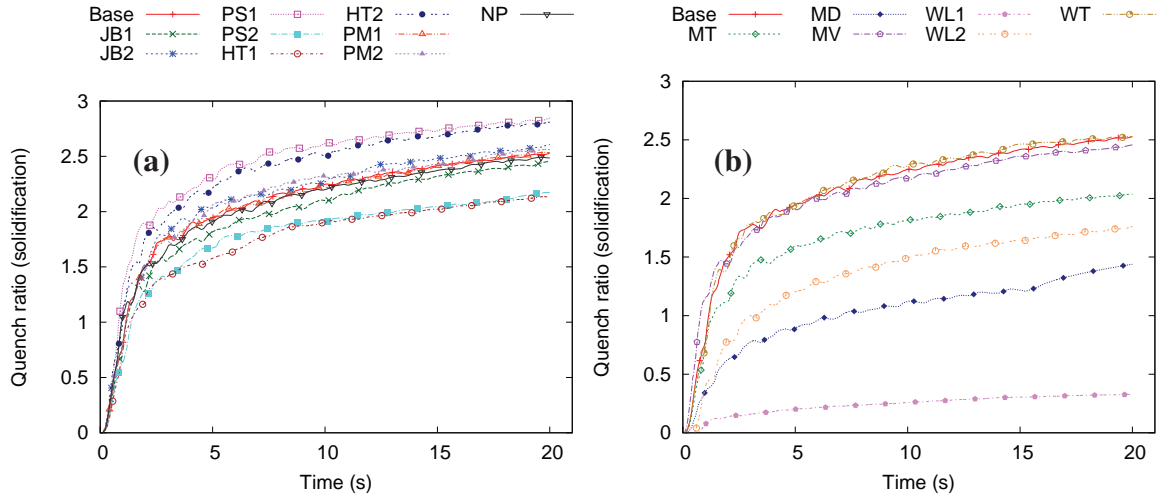


Figure 10: Quench ratio in terms of solidification, (heat exchanged)/(enthalpy for solidification); (a) influence of model parameters, (b) influence of initial/boundary conditions.

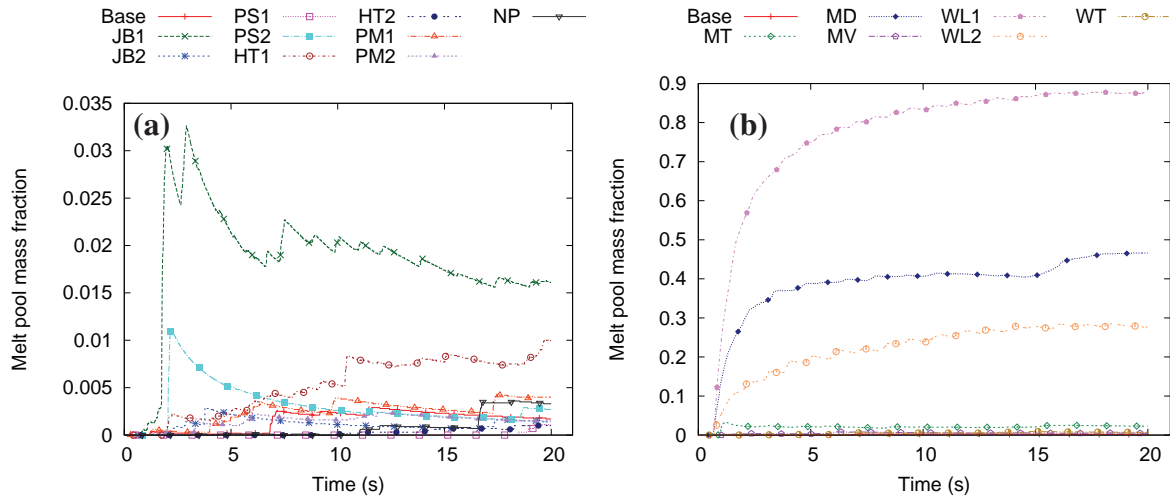


Figure 11: Melt pool mass fraction; (a) influence of model parameters, (b) influence of initial/boundary conditions.

4.4 Melt Pool Fraction and the State

Figure 11 shows the mass fraction of the melt pool, the continuous liquid or solid lump on the floor. The mass fraction of the melt pool in the base case and cases with variation of the model parameters (Fig. 11 (a)) were small, at most $\sim 3\%$ at the peak and $\sim 1.5\%$ at 20 s for the case of long jet breakup length. For the case of degraded heat transfer, HT1, the fraction was smaller but gradually increasing to the end. On the other hand, initial/boundary conditions (Fig. 11 (b)) showed strong impacts. The shallow pool cases, WL1 and WL2, and the case with large jet diameter, MD, showed much larger fraction of melt pool.

Figure 12 shows the average specific enthalpy of the melt pool relative to 300 K as base temperature. The initial phase where the mass of the pool is very small (< 1 kg) were neglected, for the heat transfer was neglected for very small amount of the pool (height < 1 mm). The line labeled “Solidus” means the enthalpy at the solidus point. The base case and most of the cases in Fig. 12 (a) showed that the pool is frozen in

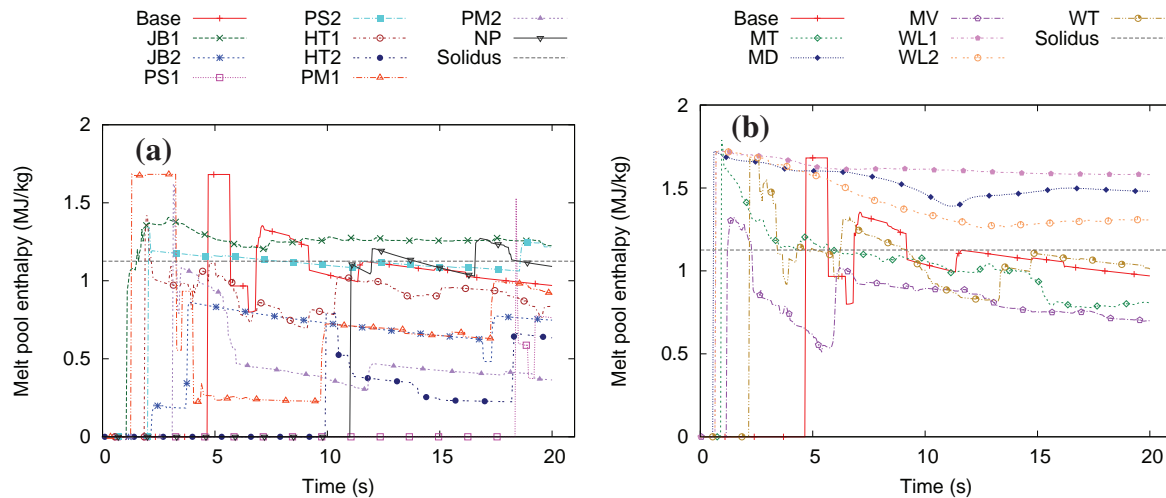


Figure 12: Melt pool specific enthalpy; (a) influence of model parameters, (b) influence of initial/boundary conditions; very small mass of the melt pool at the initial stage (<1kg) were neglected.

average at 20 s. Exceptions were the cases JB1 and PS2, longer jet breakup length and larger particle size, respectively. In Fig. 12 (b) with variation of initial/boundary conditions, the cases WL1, WL2 and MD resulted in liquid state of the melt pool at 20 s.

4.5 Comparison of the Impact of Parameters

Figure 13 compares the impact of input parameters on the results at 20 s for the quench ratios for complete quench (a) and for solidification (b), the mass fraction of the melt pool (c) and the average specific enthalpy of the melt pool (d). Each of the plots shows the value of the base case by a horizontal line. It is clear that the melt jet diameter (MD) and the water pool depth (WL1 and WL2) has major impacts and others are relatively weak.

The jet breakup length (JB1 and JB2) did not affect the heat transfer ((a) and (b)) while it was the most important among model parameters in terms of the melt pool fraction (c), though the fraction was still small ~1 %. The criterion for the particle-pool merge (PM1 and PM2), discretization criteria for particles (NP), melt jet velocity (MV) and water temperature (WT) did not affect the heat transfer ((a) and (b)), and they showed moderate impacts on the melt pool fraction (c).

The plot of the melt pool enthalpy (d) also includes the enthalpy at the solidus point for comparison. It shows that large mass fractions of the melt pool do not necessarily mean higher enthalpies, and that the cases with more than 1% melt pool fraction still in molten state (above the solidus point) at 20 s were JB1 (longer jet breakup length), MD (larger melt jet) and WL1/WL2 (shallow pool).

5 CONCLUSIONS

We applied a modified version of JASMINE code developed at JAEA, Japan, to plant scale simulation of the ex-vessel melt jet breakup and coolability. The code modifications included an empirical correlation for melt particle size distribution, non-local radiation heat transfer and improved treatment of settled particles.

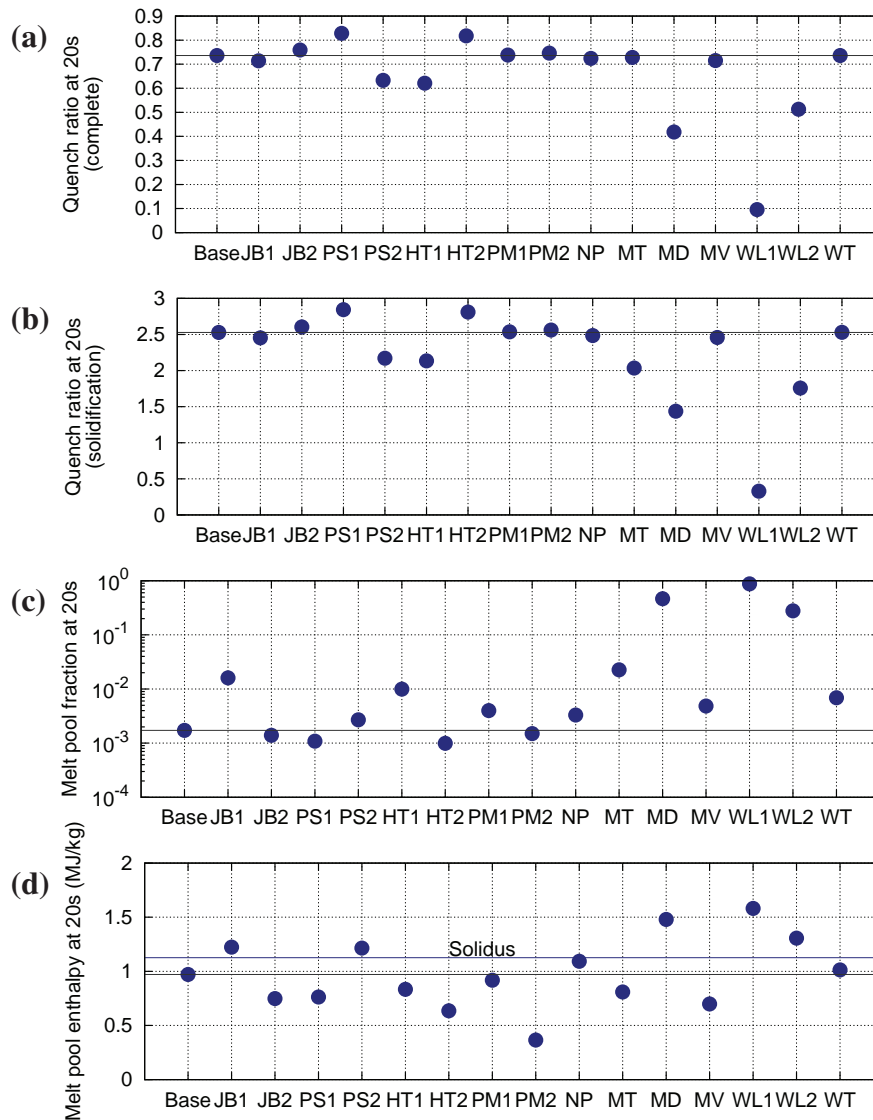


Figure 13: Impact of input parameters on the result variables; (a) Quench ratio at 20 s with basis of 300 K, (b) Quench ratio at 20 s in terms of solidification, (c) Melt pool mass fraction, (d) Melt pool average specific enthalpy.

The plant model was based on the APR1400 geometry and relevant severe accident conditions, having 145 t of molten core in the reactor vessel bottom and release of the melt as a jet into a water pool in the reactor cavity. We performed sensitivity analysis for the influence of 5 model parameters and 5 initial/boundary condition variables, in total 15 cases. Though the whole melt discharge takes a long time up to 95 s for the base case condition, the simulation results indicated a quasi steady state heat removal structure during the melt discharge. Then, we examined the results up to 20 s for the comparison between cases.

The heat removal performance was examined with the quench ratio that is the ratio of heat transferred from the melt to the enthalpy brought by the melt, in terms of the complete quench (to 300 K) or solidification. The quench ratios showed rapid development for initial 2 s and slow increase after 5 s; the latter was regarded as the quasi steady state. Also, the mass fraction and the enthalpy of the melt pool on the floor, produced by

agglomeration of the melt particles or direct arrival of the jet column on the floor was examined.

The observation are summarized as follows.

- The heat removal performance was enough for solidification, in terms of the average for the whole melt, for the base case and most of the cases, except the case with a shallow pool of 1.1 m depth.
- However, molten state of non-negligible amount ($>1\%$) of melt pool was observed in the cases of the longer jet breakup length, the larger jet diameter and the shallow water pool.
- The initial/boundary conditions had much stronger impacts on the heat removal performance and the melt pool fraction. Parameters of strong impacts were
 - water pool depth, melt jet diameter as initial/boundary conditions, and
 - jet breakup length, particle size, heat transfer coefficient as model parameters.

The assumed condition for the base case, 0.2 m diameter melt jet falling into 6 m deep water pool, resulted in breakup and quenching to solidification, with at most $<2\%$ molten pool formation considering uncertainties of model parameters, i.e. the case of longer jet breakup length. Shallower water depths less than 3 m or larger jet diameters ~ 0.5 m can cause considerable fraction of melt making molten pool on the floor.

The present result gives an insight on the state of debris bed, or melt pool, as a result of the transient melt fall and quench process. The evaluation for long term cooling against the decay heat needs another specific modeling method for such a purpose.

ACKNOWLEDGMENT

This work was supported by a grant from the Nuclear Safety Research Program of the Korea Radiation Safety Foundation, with funding by the Korean government's Nuclear Safety and Security Commission (Grant Code:1305008-0113-HD140) and by the National Research Foundation of Korea (NRF) grant funded by the Korean government (MSIP, NRF-2013M2A8A1040987)

REFERENCES

1. OECD/NEA. OECD workshop on ex-vessel debris coolability summary and recommendations. NEA/CSNI/R(2000)14, OECD/NEA/CSNI, 2011.
2. M. Bürger. Particulate debris formation by breakup of melt jets: main objectives and solution perspectives. *Nuclear Engineering and Design*, 236:1991–1997, 2006.
3. OECD/NEA. OECD research program on fuel-coolant interaction: steam explosion resolution for nuclear applications–SERENA, final report. NEA/CSNI/R(2007)11, OECD/NEA/CSNI, 2007.
4. K. Moriyama and H. Nakamura. A strategy for the application of steam explosion codes to reactor analysis. *Technical Meeting on Severe Accident and Accident Management, Tokyo, Japan, 2006*. (CD-ROM).
5. K. Moriyama, Y. Maruyama, and H. Nakamura. Steam explosion simulation code JASMINE v.3 user's guide. JAEA-Data/Code 2008-014, Japan Atomic Energy Agency, 2008.
6. K. Moriyama, H.S Park, and M.H. Kim. Simulation of melt jet breakup and coolability experiments with jasmine code. ICONE23: 23rd International Conference on Nuclear Engineering, Makuhari, Japan (ICONE23-1672). 2015.
7. K. Moriyama, Y. Maruyama, T. Usami, and H. Nakamura. Coarse break-up of a stream of oxide and steel melt in a water pool. JAERI-Research 2005-017, Japan Atomic Energy Research Institute, 2005.
8. D. Magallon. Characteristics of corium debris bed generated in large-scale fuel-coolant interaction experiments. *Nuclear Engineering and Design*, 236:1998–2009, 2006.

9. C. Liu and T.G. Theofanous. Film boiling on spheres in single- and two-phase flows. DOE/ER/12933-3, DOE/ID-10499, U.S. Department of Energy, 1996.
10. D. Magallon, I. Huhtiniemi, and H. Hohmann. Lessons learnt from FARO/TERMOS corium melt quenching experiments. *Nuclear Engineering and Design*, 189:223–238, 1999.
11. D. Magallon and I. Huhtiniemi. Corium melt quenching tests at low pressure and subcooled water in FARO. *Nuclear Engineering and Design*, 204:369–376, 2001.
12. A. Kaiser, W. Schütz, and H. Will. PREMIX: Experiments PM12–PM18 to investigate the mixing of a hot melt with water. FZKA 6380, Forschungszentrum Karlsruhe, 2001.
13. W. C. Hinds. *Aerosol Technology*. John Wiley & Sons, Inc., 1982.
14. T.N. Dinh, A.T. Dinh, R.R. Nourgaliev, and B.R. Sehgal. Investigation of film boiling thermal hydraulics under FCI conditions: results of analyses and numerical study. *Nuclear Engineering and Design*, 189:251–272, 1999.
15. L. Dombrovsky. Large-cell model of radiation heat transfer in multiphase flows typical for fuel-coolant interaction. *International Journal of Heat and Mass Transfer*, 50:3401–3410, 2007.
16. A. Annunziato, C. Addabbo, A. Yerkess, R. Silverii, W. Brewka, and G. Leva. FARO test L-14 on fuel-coolant interaction and quenching– comparison report, volume I: Analysis of the results – OECD/CSNI international standard problem 39. NEA/CSNI/R(97)31/Part I, OECD/NEA/CSNI, 1998.
17. Advanced power reactor 1400 MWe (APR1400). IAEA ARIS: Advanced Reactors Information System, <http://aris.iaea.org>, 2011.
18. J.T. Kim, S.W. Hong, R.J. Park, and S.B. Kim. A study on the hydrogen behavior and its mitigation in the APR1400 containment during a severe accident. KAERI/TR-2948/2005, Korea Atomic Energy Research Institute, 2005. [In Korean].
19. J.H. Park, H.Y. Kim, S.W. Hong, and K.S. Ha. MCCI simulation for the APR-1400 TLOFW sequence. Trans. the Korean Nuclear Society 2011 Spring Meeting, Taebaek, Korea, 2011.
20. J. Rempe, K.Y. Suh, F.B. Cheung, and S.B. Kim. In-vessel retention strategy for high power reactors. INEEL/EXT-04-02561, Idaho National Engineering and Environmental Laboratory, 2005.
21. K.I. Ahn, S.H. Park, H.D. Kim, and H.S. Park. The plant-specific uncertainty analysis for an ex-vessel steam explosion-induced pressure load using a TEXAS-SAUNA coupled system. *Nuclear Engineering and Design*, 249:400–412, 2012.
22. K. Moriyama, H.S. Park, M.H. Kim, and H. Joo. Probabilistic distribution of ex-vessel steam explosion loads influenced by the uncertainties in the initial/model parameters including water level for the case of the IVR failure in a typical PWR. NTHAS9: The 9th Symposium on Nuclear Thermal Hydraulics and Safety, Buyeo, Korea (N9P0007). 2014.